AMERICAN SCIENTIFIC PUBLISHERS
Copyright © 2014 American Scientific Publishers
All rights reserved
Printed in the United States of America

Journal of Biomedical Nanotechnology
Vol. 10, 1049–1060, 2014
www.aspbs.com/jbn

Effect of Nanostructure of Mineralized Collagen Scaffolds on Their Physical Properties and Osteogenic Potential

Yan Liu[1,†], Dan Luo[2,†], Shuai Liu[1], Yu Fu[1], Xiaoxing Kou[1], Xuedong Wang[1], Yinlin Sha[2], Yehua Gan[3], and Yanheng Zhou[1,*]

[1] *Center for Craniofacial Stem Cell Research and Regeneration, Department of Orthodontics, Peking University School and Hospital of Stomatology, Beijing 100081, P. R. China*
[2] *Single-Molecule and Nanobiology Laboratory, Department of Biophysics, School of Basic Medical Sciences and Biomed-X Center, Peking University, Beijing 100191, P. R. China*
[3] *Central Laboratory, Department of Oral and Maxillofacial Surgery, Peking University School and Hospital of Stomatology, Beijing 100081, P. R. China*

Tissue engineering has enabled development of nanostructured collagen scaffolds to meet current challenges in regeneration of lost bone. In this study, extrafibrillarly-mineralized and intrafibrillarly-mineralized collagen scaffolds were fabricated separately by a conventional crystallization method and a biomimetic, bottom-up crystallization method. Atomic force microscopy (AFM) was employed to examine the nanotopography and nanomechanics of the mineralized collagen scaffolds. The *in vitro* cell responses to the surface of the mineralized collagen scaffolds were analyzed by laser scanning microscope and field emission scanning electron microscopy. AFM imaging showed that these two mineralized collagen scaffolds exhibited different nanostructure, including the size, morphology and location of the apatites in collagen fibrils. The nanomechanical testing demonstrated that the intrafibrillarly-mineralized collagen scaffold, with bone-like hierarchy, featured a significantly increased Young's modulus compared with the extrafibrillarly-mineralized collagen scaffold in both dry and wet conditions. However, these two mineralized collagen scaffolds had a similar thermal behavior. From the cell culture experiments, the intrafibrillarly-mineralized collagen scaffold showed higher cell proliferation and alkaline phosphatase activity than the extrafibrillarly-mineralized collagen scaffold. The utmost significance of this study is that the nanostructure of the mineralized collagen scaffolds can affect the initial cell adhesion, morphology and further osteogenic potential. The present study will help us to fabricate novel biomaterials for bone grafting and tissue engineering applications.

KEYWORDS: *Nanostructure, Intrafibrillarly-Mineralized Collagen, Extrafibrillarly-Mineralized Collagen, Scaffold, Tissue Engineering.*

INTRODUCTION

Bone, as a multifunctional mineralized tissue, persistently undergoes remodeling to adapt to mechanical stress, maintain ionic balance and repair injuries. Due to the limitations of the availability and morbidity of autologous grafts, the current "gold standard" of bone substitution has been challenged.[1–3] Synthetic bone grafts,[4,5] are desirable for replacing autologous grafts but difficult for many researchers due to the complexity of bone tissue. Recently, tissue engineering (TE) offers a promising approach for repair and regeneration of bone defects by mimicking the structure and biological function of the native extracellular matrix (ECM) as much as possible in terms of both chemical composition and physical structure. The mineralized collagen fibril, as a basic building block of bone tissue,[6] is therefore believed to be an ideal candidate of TE scaffolds for bone defects because of inherent biocompatibility, biodegradability and osteoconductivity.

Type I collagen constitutes the lowest hierarchical level of bone tissue, and forms triple helical collagen molecules which self-assemble into a collagen fibril with a quarter-staggered arrangement leading to gap zones and grooves.[7] Calcium deficient nanoapatites are deposited at the intrafibrillar and extrafibrillar spaces associated

*Author to whom correspondence should be addressed.
Email: yanhengzhou@gmail.com
†These two authors contributed equally to this work.
Received: 24 May 2013
Accepted: 25 August 2013

with the collagen fibrillar self-assembly.[8–10] Understanding this intriguing process of biomineralization at the nanostructural level, many research groups have attempted to develop bone-like collagen/hydroxyapatite (HA) composites. The earlier researches mainly report on the deposition of apatite crystallites around collagen fibrils (i.e., extrafibrillar mineralization) by using conventional crystallization methods (i.e., epitaxial growth over seed crystallites).[11–17] Although these methods have successfully reproduced similar chemical composition of natural bone, they have not been able to duplicate the hierarchy of nanoapatite assembly (i.e., overlapping platelets producing periodic bands) in the mineralized collagen fibrils. As intrafibrillar mineralization has been proven to be a dominant contributor to the biomechanics of natural bone,[18–20] synthesis of mineralized collagen fibrils with intrafibrillar apatites is believed to be a key factor for mimicking natural bone nanostructure. In our previous studies, a biomimetic, bottom-up crystallization method has been applied to achieve the hierarchy of nanoapatite assembly in the mineralized collagen fibrils.[21–23] Furthermore, dramatic differences including the size, morphology and location of the apatites, have been shown between intrafibrillar mineralization and extrafibrillar mineralization.

Engineering bone tissue requires a precisely formulated combination of biomaterial scaffolds, local cell populations and growth factors. To enhance the function of the engineered tissue, the interplay between scaffolds and cells is of critical importance. It has been shown that the nanotopography, chemical composition, and physical properties of scaffolds can affect the cellular behaviors such as adhesion, morphology, migration, gene expression, proliferation, differentiation and osteogenic potential.[24–27] Therefore, we hypothesized that the mineralization method could affect the biomechanics of collagen fibrils and their cell behaviors. In the present study, the *in vitro* cell responses to the surface of the mineralized collagen scaffolds were investigated, in terms of the initial cell adhesion, morphology, proliferation and further osteogenic differentiation and mineralization.

MATERIALS AND METHODS

Fabrication of Mineralized Collagen Scaffolds

To prepare the extrafibrillarly-mineralized collagen (EMC) scaffold, a conventional crystallization method was used: Type I tropocollagen solution from rat tails (BD Biosciences, 4.05 mg/mL) contained in a dialysis membrane (3500 Da) was immersed in a flask, which contained 20 mL of simulated body fluid (SBF, 136.8 mM NaCl, 4.2 mM $NaHCO_3$, 3.0 mM KCl, 1.0 mM $K_2HPO_4 \cdot 3H_2O$, 1.5 mM $MgCl_2 \cdot 6H_2O$, 2.5 mM $CaCl_2$, 0.5 mM Na_2SO_4 and 3.08 mM Na_3N) as a phosphate source. Set Type I white Portland cement (PC, Lehigh Cement Co., Allentown, PA, USA) at the bottom of the flask released calcium and hydroxyl ion in the presence of SBF and the pH of the salts/collagen solution increased from 5 to 9.5. The HA/collagen fibrils co-precipitations were carried out at 37 °C to avoid collagen triple helices denaturation.

In the intrafibrillar mineralization system, a modified biomimetic, bottom-up crystallization method was used:[23] the tropocollagen solution was first dialyzed by sodium tripolyphosphate (TPP, 2.5 wt%, Mw 367.9, Sigma-Aldrich) to template hierarchical arrangement of nanoapatites within collagen fibrils. And poly(acrylic acid) (PAA, 0.28 mM, Mw 1800, Sigma-Aldrich) was added to SBF to mimick the role of specific soluble proteins stabilizing amorphous calcium phosphate (ACP) as a nanoprecursor. The dialysis membrane containing the mineralized collagen fibrils was then immersed in a phosphate buffer saline (PBS, 0.1 M).

Characterization of Mineralized Collagen Scaffolds

Atomic Force Microscopy (AFM)

The surface nanotopography of the collagen fibrils was obtained by AFM imaging. Briefly, the fibrillized collagen at a concentration of 10 μg/mL was collected on freshly-cleaved muscovite mica disks (grade V1, Ted Pella Inc.). The samples were flushed thrice with deionized water in multiple flow directions. Excess water from the edges of the mica disks was carefully removed by Kimwipes. The samples were then left to air-dry for more than 10 min and half-covered with a plastic dish. AFM imaging was performed with a MultiMode IV scanning probe microscope (SPM, Veeco, USA), in tapping mode with silica tips (spring constant 40 Nm^{-1}, frEq. 300 kHz, RTESP, Veeco, USA) in ambient conditions (uncontrolled humidity, temperature, and air pressure). The scanning speed was between 0.3 and 0.5 Hz, with a 0° scan angle. Image analysis and processing were performed with the NanoScope™ Analysis software version 6.12.

Nanomechanical Measurements in Dry and Wet Station

Quantitative nanomechanical characterizations were determined using Bruker MultiMode 8 SPM, operated under the peak-force tapping mode with 1.0 Hz scan rates and 200 mV amplitude set point.[28] The measurements were performed both in ambient conditions and in physiological buffer (10 mM Tris-HCl, 50 mM NaCl, pH 7.4). For the ambient measurements, the stiff RTESP cantilevers (spring constant 25.89 Nm^{-1}, Veeco, USA) were used, due to the high adhesion forces observed for other, less stiff cantilevers. For the measurements performed in buffer, we used a medium stiff cantilever with a spring constant of 0.975 Nm^{-1} (SCANASYST-FLUID, MultiMode 8, Catalyst, Icon). To calculate Young's modulus, the retract curve of force versus separation plots could be fitted by a Derjaguin–Muller–Toporov (DMT) model.[29]

Field Emission Scanning Electron Microscopy (FE-SEM)

The morphology of the collagen nanofiber scaffolds fixed on polylysine-coated glass coverslips was observed by FE-SEM (Hitachi S-4800, Japan). For cell-seeded scaffolds, they were previously washed thrice with PBS and fixed in 2.5% glutaraldehyde in PBS. All the samples were dehydrated in graded series of ethanol (50, 70, 80, 85, 90, 95 and 100%), critical-point dried, and observed under FE-SEM at 15 kV.

Thermogravimetric Analysis and Differential Scanning Calorimetry (TGA/DSC)

The mineralization degree of the collagen scaffolds was determined by TGA/DSC (SDT Q600, TA Instruments, USA) in an air atmosphere (100 mL/min). Briefly, the dense fibrillized collagen with concentration of 4.05 mg/mL was collected by centrifugation for 10 min at 3000 rpm and filled in the cavities of a 24-well polystyrene plate. After freeze-drying, sponge-like porous scaffolds were achieved. The lyophilized collagen scaffolds were cut into small pieces and about 10 mg of samples were used for examination. The measurement was performed from room temperature to 800 °C with a heating rate of 10 K/min.

Cell Culture

The human osteoblast-like MG 63 cell line (ATCC, Rockville, MD) was cultured in Alpha Modification of Eagles Medium (α-MEM) supplemented with 10% fetal bovine serum (FBS), 100 U/mL penicillin and 100 μg/mL streptomycin. The fibrillized collagen at a concentration of 2 mg/mL was collected on polylysine-coated glass coverslips of 15 mm diameter, and cross-linked with 1-ethyl-3-(3-dimethylaminopropyl)-carbodiimide (0.3 M)/*N*-hydroxysuccinimide (0.06 M) to stabilize the scaffolds.[21] The glass coverslip was used as a control. Then, the collagen nanofiber scaffolds were placed in a 24-well non-treated polystyrene plate with a stainless steel ring to prevent swelling. Before cell seeding, all the samples were sterilized under ultraviolet light for 2 h, and washed with PBS for 15 min each to remove any residual solvent, and subsequently immersed in complete medium (α-MEM/10% FBS/100 U/mL penicillin/100 μg/mL streptomycin) overnight. After reaching near-confluence, MG 63 cells were detached and seeded on the scaffolds at a cell density of 2×10^4 cells per well.

Cell Assays

Cell Proliferation

The number of living cells on different substrates was estimated using CellTiter 96 Aqueous One Solution (Promega, Madison, WI, USA) at determined time points. Nine replicates were used for each substrate and all experiments were repeated at least once. Briefly, the medium was aspirated and the samples were washed thrice with PBS. Then, the samples were incubated in a 1:5 ratio mixture of 3-(4,5-dimethylthiazol-2-yl)-5-(3-carboxymethoxyphenyl)-2-(4-sulfophenyl)-2H-tetrazolium (MTS) assay and serum-free α-MEM medium for 3 h at 37 °C. After the incubation period, the samples were pipetted out into 96 well plates and the absorbance was read at 490 nm using a microplate reader (Bio-Rad, Japan). The background absorbance value of blank MTS-α-MEM was subtracted from all wells. A calibration curve of MG 63 cells was established to estimate the number of living cells from the absorbance index.

Alkaline Phosphatase (ALP) Activity

To determine ALP activity at different time points, an independent experiment was performed. After 24 h of cell cultivation on different substrates, the complete medium was supplemented with 10^{-7} M dexamethasone, 10 mM β-glycerophosphate and 0.05 mM ascorbic acid 2-phosphate. ALP activity was determined by a colorimetric method using an Alkaline Phosphate Yellow Liquid substrate for ELISA (Sigma-Aldrich) ($n = 9$ culture wells).[26,30] Briefly, after aspirating the medium from culture wells and rinsing thrice with PBS, 400 μL of ALP substrate was added into each well. After incubation for 30 min at 37 °C, the reaction was stopped by adding 100 μL of 3 N NaOH into each well. Quantification was performed with the microplate reader at 405 nm. The optical density of blank ALP-NaOH was subtracted from all wells.

Immunohistochemistry

Cellular morphology and adhesion were investigated by examining the F-actin to label the cytoskeleton arrangement and vinculin to label focal adhesion points (FAPs) respectively. After being cultured for 6 h, the cells were fixed with 4% formaldehyde for 10 min, permeabilized with 0.2% Triton-X-100® and incubated with anti-vinculin antibody (Clone hVIN1, #V9264, Sigma-Aldrich) at a 10 μg/mL final concentration for 1 h. The cells were then rinsed and incubated with Alexa Fluor 488 Phalloidin (Sigma-Aldrich) and Alexa Fluor 647 Goat anti-Mouse IgG (Sigma-Aldrich) at 2 μg/mL for 45 min. After washing thrice with PBS, the cells were mounted with mounting media containing 4′,6-diamidino-2-phenylindole (DAPI) for nuclei staining.

The osteogenic differentiation of MG 63 cells was confirmed using immunofluorescent staining by employing osteoblast specific marker protein, osteocalcin (OCN). On day 5 of the cell culture study, cells were fixed and incubated with osteoblast specific marker protein OCN (abcam, USA) in the dilution 1:100 for 90 min at room temperature. Cells were then rinsed and incubated with Alexa Fluor® 488 Phalloidin and Alexa Fluor® 647 Goat anti-Mouse IgG. After washing, cells were mounted with mounting media containing DAPI. Confocal microscopic images were acquired using a Zeiss laser scanning

microscope (LSM 510) and analyzed by LSM 5 Release 4.2 software.

Alizarin Red S Staining

The amount of ECM secreted by MG 63 cells was analyzed by Alizarin red S staining. After aspirating the medium, the samples were rinsed thrice with PBS and fixed with 4% formaldehyde for 10 min. The fixed samples were subsequently rinsed thrice with deionized water and stained with 2% Alizarin red S (Sigma-Aldrich) for 20 min at room temperature. After several washes with deionized water, the scaffolds were visualized under a light microscope.

Statistical Analysis

To calculate Young's modulus, 2 scans were performed for each sample and 10 Regions of Interest (ROIs) were selected at each scan. A median value was used to represent the property value for that ROI. Then, the generated values (2 scans $\times$ 10 ROIs $\times$ 5 samples) in each group were expressed as means $\pm$ standard deviation (SD). As normality (Shapiro-Wilk test) and homoscedasticity assumptions (modified Levene test) of the data for each parameter were violated, statistical analysis was performed by Kruskal-Wallis one-way ANOVA at $\alpha = 0.05$.

RESULTS

Nanotopography and Nanomechanics of Mineralized Collagen Fibrils

The tropocollagen solutions (10 μg/mL) assembled for 24 h under different conditions were used for AFM tests (Figs. 1 and 2). Without PC (i.e., only SBF), collagen molecules self-assembled into fibrils (158.2 $\pm$ 29.3 nm) with distinct D-periods (*ca.* 67 nm) and then the fibrils aggregated longitudinally and laterally with adjacent fibrils to form cross-banded nanofibers (387.6 $\pm$ 19.1 nm) with 67 nm periods (Figs. 1(A) and (B)). When the conventional crystallization method was applied (i.e., SBF and PC), big apatite clusters randomly arranged around the nanofibers (Figs. 1(C) and (D)). Conversely, in the presence of two biomimetic analogs in the mineralization medium (i.e., PAA and TPP), hierarchically, intrafibrillarly-mineralized collagen (IMC) fibrils were formed (Fig. 1(E)). As shown in Figure 1(E) with high magnification, nanoapatites were regularly arranged within the collagen fibrils and nanofibers, with the distance between two adjacent nanoapatites identical to 67 nm or multiplies of 67 nm (data not shown).

The AFM-based PeakForce Quantitative Nanomechanical Mapping (QNM) technique was employed to study the variation in mechanical properties of the mineralized collagen fibrils. Figure 2 showed a comparison of elastic modulus on mineralized collagen fibrils in both dry and rehydration conditions. The modulus of the unmineralized collagen (Col) fibrils in dry station ranged from 0.2 GPa to 7.8 GPa, which was much lower than that

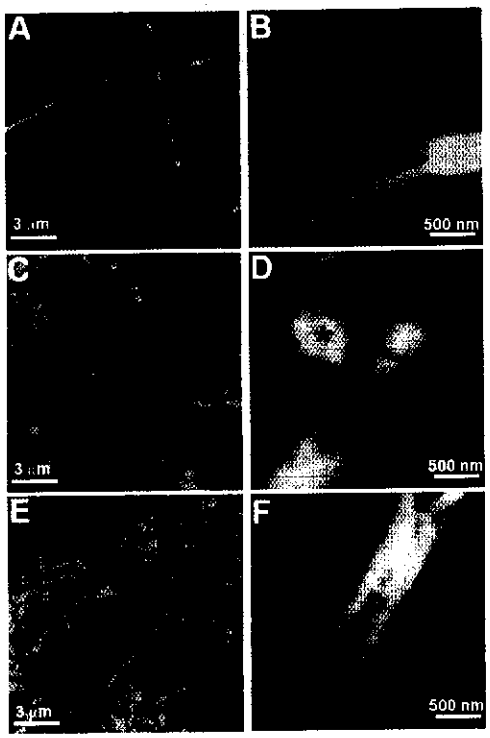

Figure 1. Collagen fibrils assembled for 24 h and observed by AFM. (A), (B) Col. Cross-banded fibrils (*ca.* 138 nm, open arrowhead) assembled into nanofibers (*ca.* 500 nm, arrows). (C), (D) EMC. Flower-like apatite clusters (stars) deposited around fibrils or nanofibers (arrows). (E), (F) IMC. Nanoapatites regularly arranged in the fibrils (*ca.* 105 nm) and formed obvious D-periods (*ca.* 67 nm) (open arrowheads). Arrows: mineralized fibrils assembled into nanofibers or bundles (*ca.* 210 nm) showing distinct *D*-periods.

of the mineralized collagen (i.e., EMC and IMC) fibrils ($p < 0.05$). Compared with EMC, with a modulus of 7.1 $\pm$ 1.9 GPa, the modulus of IMC (13.7 $\pm$ 2.6 GPa) was much higher ($p < 0.05$). As natural bone is a hydrated hard tissue composed of approximately 10 wt% of water,[31] it is important to evaluate the mechanical properties of the mineralized collagen fibrils in the fully hydrated condition. In this study, both Col (19.5 $\pm$ 6.5 MPa) and EMC (116.6 $\pm$ 28.4 MPa) suffered a severe reduction in modulus after rehydration ($p < 0.001$). When the IMC fibrils was rehydrated, it also showed much lower modulus (2.6 $\pm$ 1.5 GPa) than in dry station, but significantly higher mechanical properties were assessed in comparison with the Col and EMC fibrils. The significant reduction in modulus in the wet station of all the collagen fibrils is probably triggered by the high quantities of incorporated water.

Micrographs of Mineralized Collagen Scaffolds

The mineralized collagen nanofiber scaffolds prepared from highly concentrated fibrillar suspensions (2 mg/mL) were tested for their ability to support cell growth and differentiation *in vitro*. Before cell seeding, the morphology of the scaffolds was observed by FE-SEM to ensure

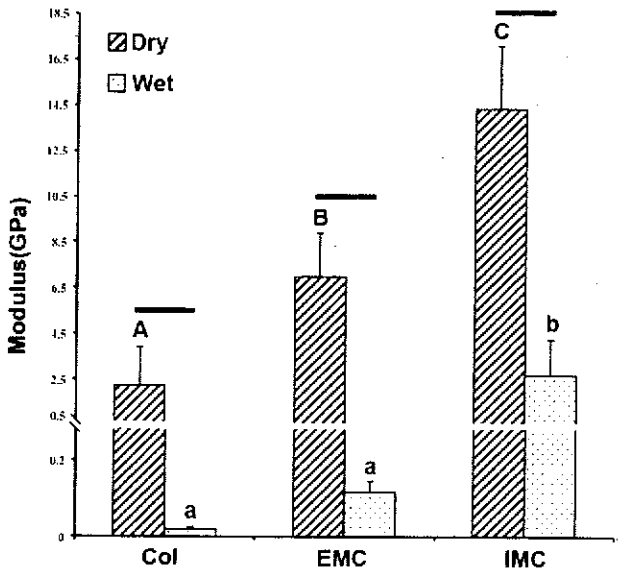

Figure 2. Nanomechanical measurements of the mineralized collagen fibrils in dry and wet condition. For the dry subgroups, columns with different upper case letters are significantly different ($p < 0.05$). For the wet subgroups, columns with the same lower case letters are not significantly different ($p > 0.05$). For each mineralized group, different condition connected by a black horizontal bar are significantly different ($p < 0.05$).

uniform coverage of nanofibers on the glass coverslips. As shown in Figure 3, the collagen scaffold exhibited different morphology and only the Col nanofibers collapsed after vacuum. For EMC scaffold, flower-like apatites deposited over the surface of nanofibers; while no extrafibrillar apatite was found in the IMC nanofibers. Furthermore, the presence of an intrafibrillar apatite mineral phase in the IMC scaffold, which increased the diameter of the collagen nanofibers, was confirmed using energy dispersive X-ray spectroscopy (EDS) coupled to FE-SEM. The micrographs of the mineralized collagen nanofibers were consistent with their surface nanotopography observed by AFM.

Calorimetry Results

The TGA curves of the collagen scaffolds were shown in Figure 4(A). A mass loss about 10% of all the samples occurred before 200 °C, which can be attributed to the evaporation of physisorbed water.[32] After 200 °C, the mass of the Col scaffold continued to lose, while the mass of the EMC and IMC scaffolds almost kept stable until 260 °C. DSC measurements also showed that the Col scaffold began to decompose at 210 °C (Fig. 4(B)). This result demonstrated that the mineralized collagen had a higher thermal stability than the pure collagen.[33] When the

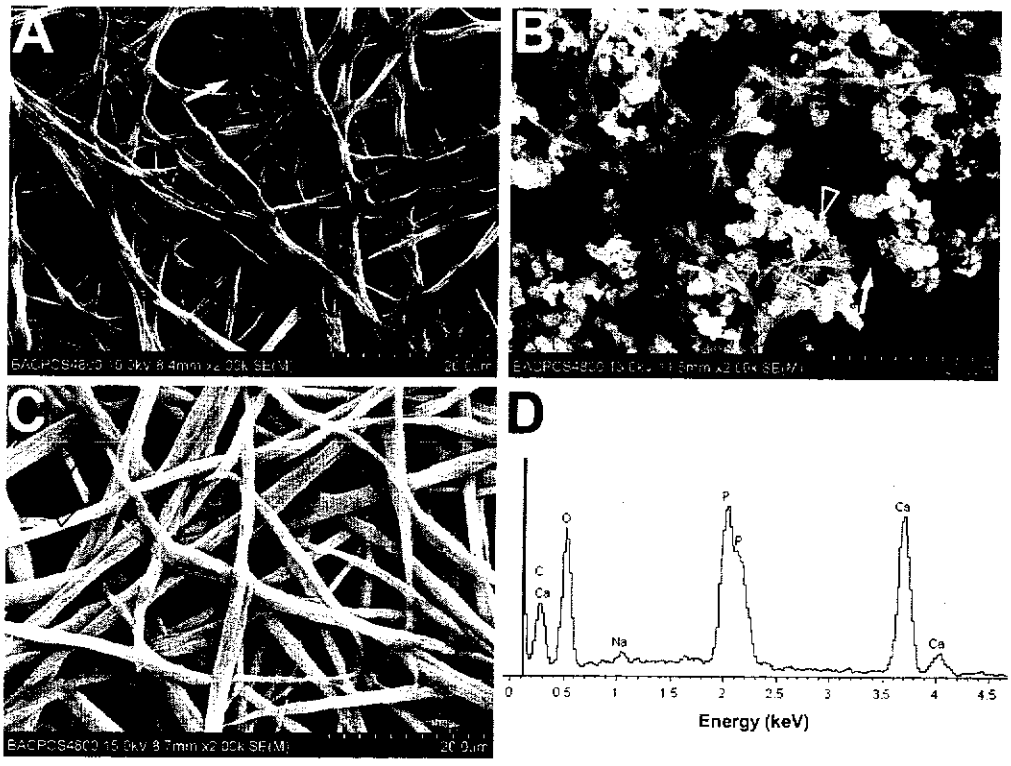

Figure 3. FE-SEM micrographs of the collagen scaffolds treated for 72 h. (A) Col. The unmineralized nanofibers shrunk and collapsed under dehydrated condition (arrow). (B) EMC. Flower-like, spherulitic aggregates (open arrowhead: *ca.* 2 μm in diameter) deposited around nanofibers (arrow). (C) IMC. Under auto-contrast, the nanofibers with increased diameter had similar electron density to the flower-like apatites in B. Open arrowheads: brittle fracture. (D) EDS analysis, confirming an intrafibrillar calcium phosphate mineral phase (Ca/P = 1.6) in C.

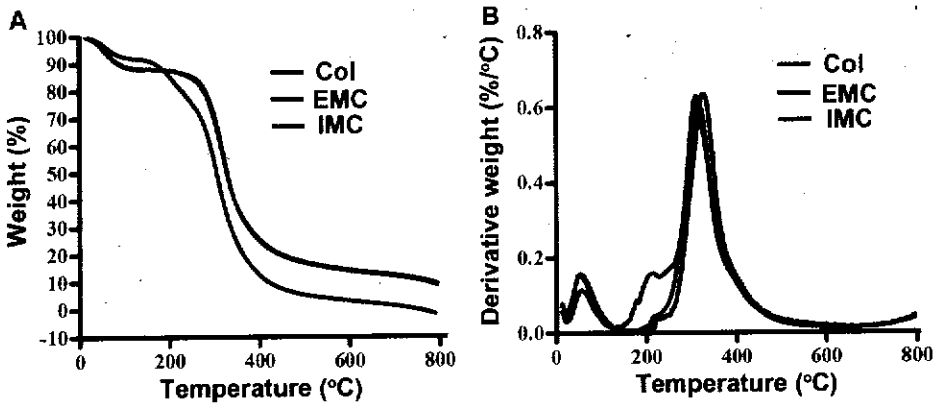

Figure 4. TGA/DSC of different collagen scaffolds. (A) TGA curves of the Col, EMC and IMC scaffolds. The residual mass of the mineralized collagen scaffolds corresponded to inorganic material around 700 °C. The small weight loss beyond this temperature was attributed to CO_2 loss from carbonated apatite. (B) DSC thermograms of the Col, EMC and IMC scaffolds. The thermal decomposition of the mineralized collagen scaffolds was at a temperature of around 320 °C.

temperature increased to 700 °C, the residual mass of the EMC (12.1%) and IMC (12.4%) scaffolds was almost the same. The large mass loss in both the EMC (72.1%) and IMC (70.9%) scaffolds occurs corresponding to the degradation of organic residues such as collagen from 260 °C to 700 °C.[34] Combined with DSC curves, the EMC and IMC scaffolds exhibited a similar thermal behavior. The strong exothermic peaks of the mineralized collagen scaffolds in DSC curves at about 320 °C corresponded to collagen decomposition, which is comparable to native bone.[35]

Biochemical Assays

Cell growth on different substrates was quantified using a colorimetric MTS test. Figure 5(A) showed the cell number in different substrates increased significantly with the cultivation time. Compared with the Col and EMC scaffolds, the IMC scaffold had a better cell compatibility to MG 63 cells on days 1 and 3 ($p < 0.05$). However, the number of cells on different collagen scaffolds was similar on day 7 ($p > 0.05$). This result indicates that the cells on the different collagen scaffolds reached confluence and began to differentiate along an osteogenic lineage. Cell numbers for the control group at different time points were lower than those on different collagen scaffolds.

ALP activity, as an early marker of cell osteogenic differentiation, was affected in a similar manner, with cells on the coverslip having lower levels of enzyme activity than cells on different collagen scaffolds. As shown in Figure 5(B), a considerable increase in ALP activity was observed in different substrates and from day 1 to day 7 ($p < 0.05$). Similar to the cell proliferation, the IMC scaffold showed significant higher ALP activity than the EMC scaffold at different time points ($p < 0.001$). ALP activity of MG 63 cells cultured under osteogenic conditions usually peaks after 14–21 days, depending on culture conditions. In this study, the percentage increase in the rate of proliferation on all scaffolds from day 3 to day 7 was much higher than that from day 1 to day 3 ($p < 0.05$). This finding may indicate ALP activity of differentiated MG 63 cells did not reach the maximum level.

Cell Morphology

The morphology of MG 63 cells cultured on different substrates were indicated by F-actin staining (green) (Fig. 6).

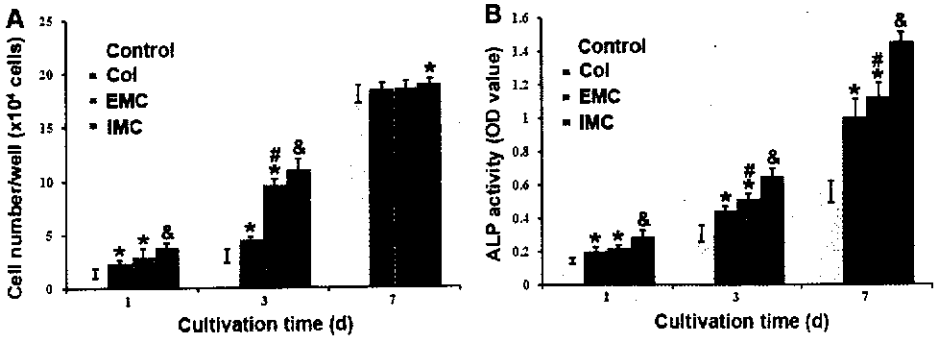

Figure 5. Proliferation and differentiation of MG 63 cells determined by MTS (A) and relative ALP activity analysis (B). Cells were cultured on different substrates. Values were expressed as means ± SD ($n = 9$). The statistical differences were determined using ANOVA variance at $\alpha = 0.05$. *: $p < 0.05$ versus control; #: $p < 0.05$ versus Col; &: $p < 0.05$ versus all of the other groups.

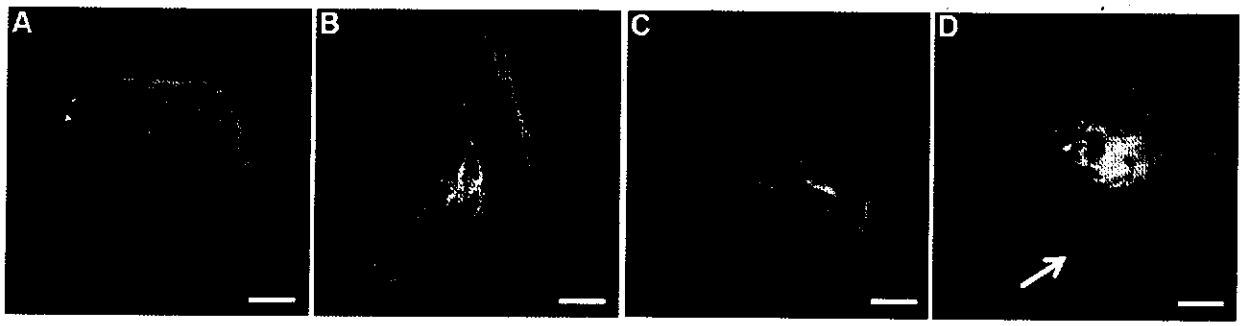

Figure 6. Fluorescent microscopic micrographs of MG 63 cells cultured on the glass coverslip (A), Col (B), EMC (C) and IMC (D) scaffolds for 6 h. Cells cultured on the IMC scaffold spread well and showed high adhesion, even at the edge of the cell (arrow). Triple labeling includes Alexa Fluor 488 Phalloidin (green), anti-vinculin (red) and DAPI (blue). Scale bar = 10 μm.

Besides, focal adhesions in the cell-scaffold interface were stained simultaneously (red). Most of the cells adhered to the scaffolds after a 6 h attachment period and appeared to be spread. Compared with the cells cultured on the Col scaffold, the cells cultured on the mineralized collagen scaffolds showed more filopida and higher density of FAPs, especially the cells cultured on the IMC scaffold. Moreover, the FAPs on the surface of the IMC scaffold appeared to be distributed on the whole cell surface, even extend to the cell periphery. While in the EMC scaffold, the FAPs were more concentrated in the center of the cell.

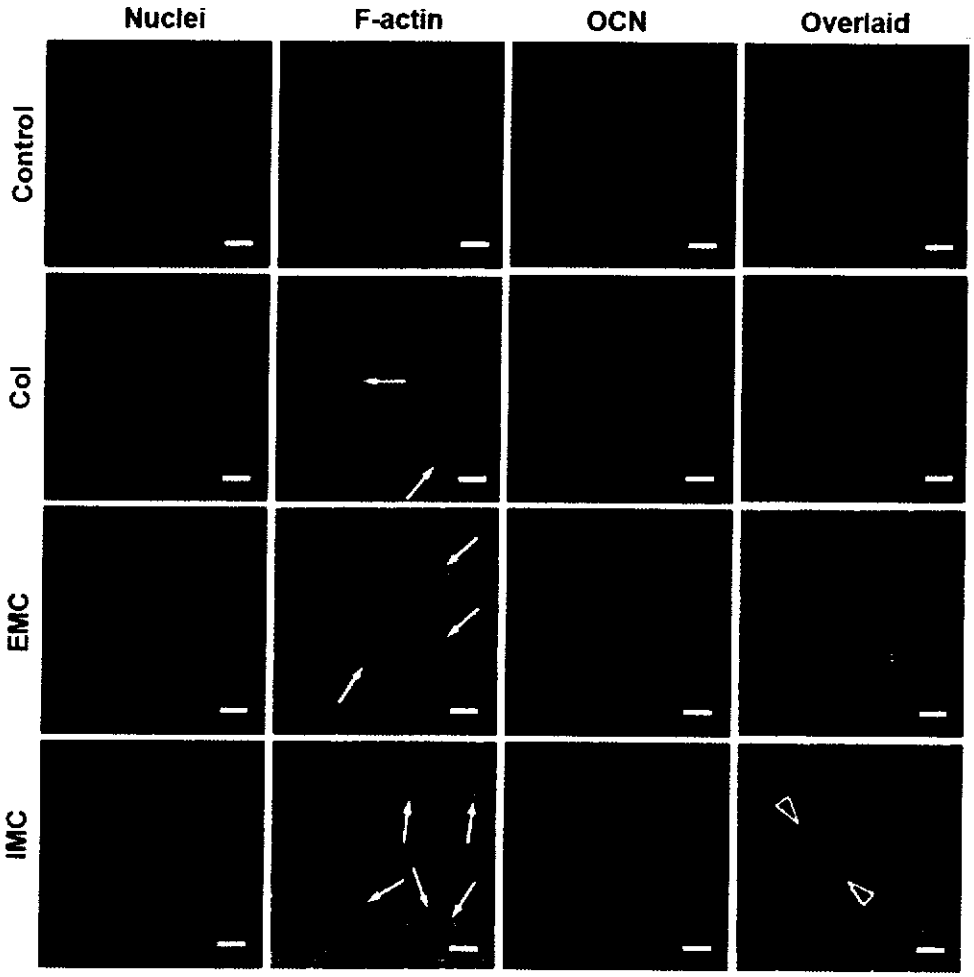

Figure 7. OCN and actin cytoskeleton staining of MG 63 cells on the glass coverslip, Col, EMC and IMC scaffolds in the osteogenic medium after 5 days. Cells cultured on the IMC scaffold had the highest OCN density and the most stress fibers (arrows). Open arrowheads indicated the characteristic cuboidal morphology of osteoblasts. Scale bar = 20 μm.

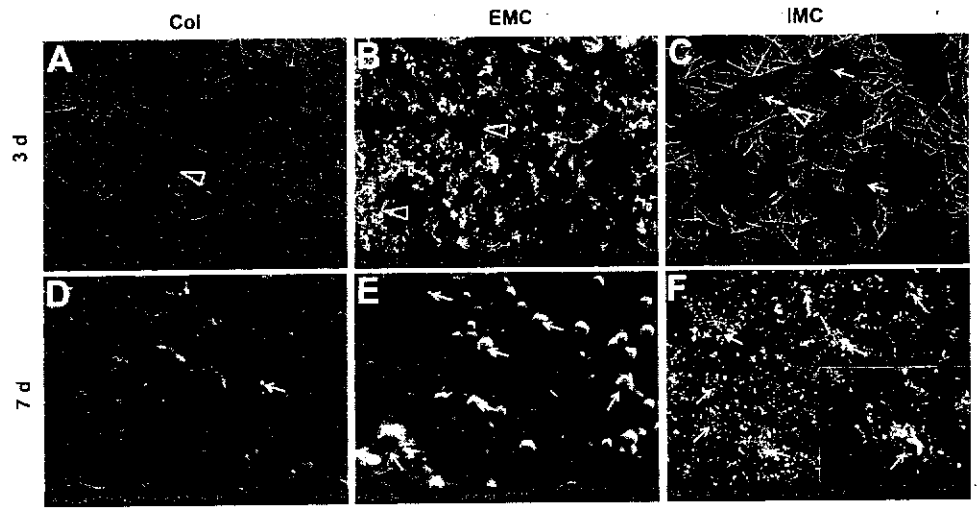

Figure 8. FE-SEM images showing the cell-scaffold interactions on the Col (A), (D), EMC (B), (E) and IMC (C), (F) nanofibers on day 3 and 7 after cell seeding. Arrows: bone nodules. Open arrowheads: extensive filopodia.

OCN Staining

As a bone specific protein, OCN is preceded by ALP in the differentiation process. In this study, the osteogenic differentiation of MG 63 cells on different collagen scaffolds was confirmed by performing immunostaining analysis using OCN (Fig. 7). In comparison with the Col scaffold, higher density of OCN (red) was shown on the surface of mineralized collagen scaffolds, owning to the increased cell adhesion, proliferation and ALP activity in the presence of apatites. Between these two mineralized collagen scaffolds, the OCN expression on the IMC scaffold was more than that on the EMC scaffold. Additionally, the reorganization of actin filaments (green) was also pronounced in the IMC scaffold, where concentrated intertwined stress fibers formed at the cellular periphery (Fig. 7). More importantly, the cells cultured on the IMC scaffold exhibited the characteristic cuboidal morphology of osteoblasts.

Matrix Mineralization

The cell-scaffold interactions were observed by FE-SEM on day 3 and 7 (Fig. 8). On day 3, the filopodia were observed to be in direct contact with neighboring cells as well as with the underlying collagen scaffolds. A few of bone nodules were identified on both the EMC and IMC scaffolds at this time, as indicated by arrows (Figs. 8(B) and (C)). After 7 days, the surface of the collagen scaffolds appeared to be completely covered with multi-layers of cells as well as cell secreted ECM (Figs. 8(D)–(F)), indicating confluence of MG 63 cell growth. Furthermore, the secretion of ECM scaffold occurred on the mineralized

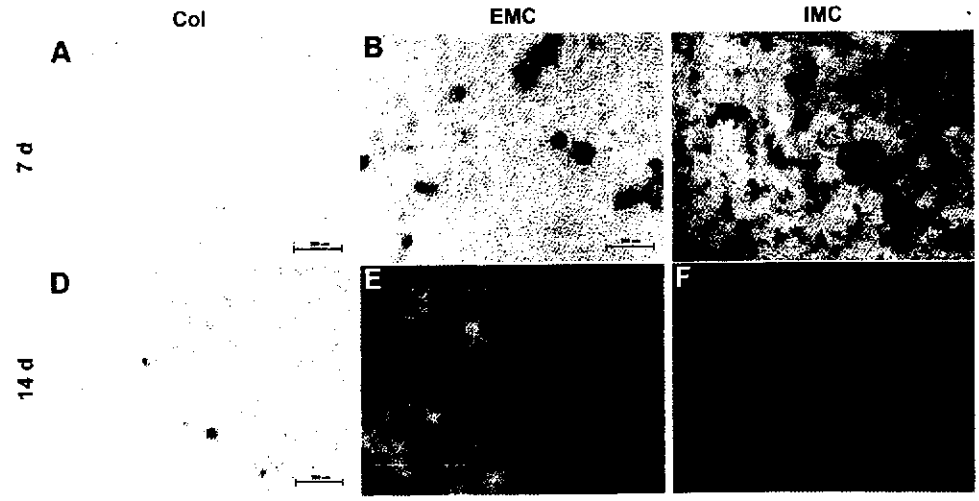

Figure 9. Alizarin red S staining of MG 63 cells differentiated on different collagen scaffolds in the osteogenic medium on day 7 (A)–(C) and 14 (D)–(F). The IMC scaffold had remarkably higher calcium amounts than the Col and EMC scaffolds.

collagen scaffolds was principally apatites in the form of globular accretions. Notably, the cells cultured on the IMC scaffold produced more bone nodules than the ones on the EMC scaffold. The presence of inorganic atoms in the bone nodules was confirmed by EDS, with the Ca:P ratio of approximately 1.42 (data not shown).

The mineralization of the ECM on the collagen scaffolds was also illustrated by Alizarin red S staining, in which the mineral deposition was stained with orange-red spots. As shown in Figure 9, the amount of mineral deposits on the collagen scaffolds increased from day 7 to day 14. More importantly, compared with the Col and EMC scaffolds, the IMC scaffold were apparently in favor of producing much more minerals, as observed by FE-SEM.

DISCUSSION

Nanomaterials such as polymeric/inorganic nanoparticles, nanofibers and nanotubes are widely used as scaffolds for cell growth[36]and delivery vehicles for various drugs,[37–39] growth factors,[40–43] and gene related peptides,[44,45] in TE. Recently, electrospun polymeric nanofibers derived from poly(L-lactic acid),[26,39] polycaprolactone,[46–48] poly(vinyl alcohol),[48–50] or poly(D,L-lactic-co-glycolic acid)[51] have attracted extensive attention in bone TE due to their capability to provide the support necessary for cells to grow and differentiate into a functional tissue. However, scaffolds derived from natural polymers (i.e., collagen) offer greater bioactivity and biocompatibility with bone tissue to favor tissue regeneration, owing to their similarity to native ECM components.[24–25,52] Furthermore, it has been shown that through the electrospinning process, collagen denatures and lacks the unique ultra-structural axial periodicity.[53] This appears to defeat the purpose to create biomimetic scaffolds emulating the collagen structure and function of the ECM in TE. In the present study, the collagen scaffolds were fabricated by self-assembly process and showed distinct D-periods similar to natural collagen (Fig. 1).

Structurally and biologically to duplicate a functional, engineered bone tissue, it is important to design scaffolds with nano- and micro-sized architecture similar to that of native bone. In this study, two types of mineralized collagen scaffolds were produced by different crystallization approaches. These two mineralized collagen scaffolds exhibited different nano- and micro-morphology as shown in Figures 1 and 3. The IMC scaffold, fabricated by the biomimetic, bottom-up crystallization approach, showed bone-like hierarchical nanostructure. This may be attributed to the important role of dual sequestration (i.e., PAA) and nucleation (i.e., TPP) analogs of non-collagenous proteins in recapitulating the hierarchical apatite arrangement within collagen fibrils.[54] However, when using the conventional crystallization approach, large, flower-like apatites were randomly deposited around the collagen in the EMC scaffold. This result is similar to previous studies.[11–17]

The recently developed PeakForce QNM technique, which is beneficial for soft delicate biological specimens,[55] was applied to examine the nanomechanics of collagen fibrils in both dry and wet station. To decrease scan artifacts and additional experimental constraints such as thermal drift in the wet condition,[56] we used the stiff cantilever with much lower spring constant. As shown in Figure 2, the IMC scaffold, with hierarchical intrafibrillar nanoapatite assembly, possessed the highest modulus compared with the Col and EMC scaffolds. The mechanism may be that the nanocrystalline apatites substitute water in the gap zones between the collagen molecules and establish intermolecular chemical interactions between the organic and mineral phase.[57] The higher modulus of the IMC scaffold than the EMC scaffold is similar to what is shown in natural bone: the mechanical property mainly depends on the intrafibrillar apatites within the gap zones of the fibrils, even though the extrafibrillar apatites constitute as much as 75% of the mineral phase in mineralized collagen.[58,59]

Mineralization has been proved to be an effective method to protect collagen from degradation.[60–63] In this study, the mineralization of collagen strongly altered its thermal behavior as shown in Figure 4. This phenomenon has also been observed for collagen in bone and dentin.[35] Furthermore, the TGA/DSC measurements confirmed the preventive role of minerals in collagen decomposition, which may be attributed to the intimate structural relationship between apatites and collagen fibrils.[64] Based on this interpretation, the TGA/DSC examination can be used as a supplementary means for identification of intrafibrillar apatites in collagen fibrils in FE-SEM test.

As is well known, bone formation is a complex sequence of events that begins with the recruitment and proliferation of osteoprogenitor cells followed by cellular differentiation, osteoid formation and ultimately mineralization.[65] In the present study, osteoblast-like MG 63 cells were used to examine their osteogenic activity in the mineralized collagen for a bone TE scaffold. As initial attachment of the MG 63 cells is especially critical for their long-term stability and differentiation, the capacity for the mineralized collagen scaffolds to support the cell adhesion and proliferation was evaluated using MTS assay as shown in Figure 5. The higher cell number on the IMC scaffold may be attributed to their smooth surface topography and advanced mechanical properties. As a marker of early osteoblastic differentiation, the ALP activity was tested after cell seeding on days 1, 3, and 7. Elevated levels of ALP activity were noticed on the two mineralized collagen scaffolds. This may be because of the important role of mineral apatites in inducing *in vitro* osteoblastic differentiation of precursor cells as well as enhancing *in vivo* bone formation.[66–67] However, the ALP activity on the IMC scaffold was significantly higher than that on the EMC scaffold. This may be due to nano-sized apatites in the IMC scaffold.[68–69] Similar result was found in the expression of OCN, which is believed to play a significant role

in regulating mineralization and bone formation.[70] Taken together, these findings indicated the great advantages of the IMC scaffold in osteogenic differentiation of MG 63 cells.

Upon undergoing osteogenic differentiation, the cells begin to secrete mineral matrix, which was determined by FE-SEM and ARS staining. In comparison with the Col scaffold, the two mineralized collagen scaffolds were apparently in favor of producing much more mineral deposits in the form of globular accretions (Fig. 8), as reported in previous studies.[71,72] Due to the nanostructure of the IMC scaffold mimicking the ECM nanostructure, the IMC scaffold provide a micro-environment more similar to the native ECM *in vivo* than the EMC scaffolds. Therefore, compared to the EMC scaffold, ARS staining was significantly higher on the IMC scaffold on day 7 and 14, due to the bone-like hierarchical nanostructure which enhances mineral deposition (Fig. 9). The ability to produce a high mineral deposition is a good evidence for the potential of the IMC scaffold *in vivo*.

The cell-scaffold interactions not only depend on chemical composition but also the physical properties of the scaffolds. In this study, the morphology of the cells cultured on the IMC scaffold was different from those cultured on the EMC scaffold as indicated by actin cytoskeleton and focal adhesion staining in Figure 6. Compared with the cells seeded on the EMC scaffold, the cells seeded on the IMC scaffold showed more filopida and a more elongated shape. This reorganization of actin filaments might derive from the higher density of FAPs shown on the IMC scaffold, as focal adhesion plays an important role in linking the ECM on the outside to the actin cytoskeleton on the inside at the cell-matrix interface.[73] These results, together with the cell number, ALP, OCN and mineralization data, suggest that the IMC scaffold with bone-like hierarchical nanostructure exhibited great advantages in cellular behavior.

CONCLUSIONS

In summary, the two mineralized collagen scaffolds, synthesized by the conventional crystallization method and the bottom-up crystallization method separately, exhibited different nanotopography and nanomechanics. The IMC scaffold, with bone-like hierarchical nanostructure, showed enhanced nanomechanical properties compared with the Col and EMC scaffolds in both dry and wet conditions. From TGA/DSC measurements, mineralization could protect collagen from decomposition, and the effect of the mineralization method on the collagen's thermal behavior was comparable. However, the *in vitro* cell assays demonstrated that the nanostructure of the mineralized collagen scaffolds could influence their biological activities, such as initial cell adhesion, morphology, proliferation and further osteogenic differentiation and mineralization. Future research should be directed toward *in situ* hard tissue regeneration by fabrication of more densely packed 3D collagen scaffolds with hierarchical, intrafibrillar nanoapatite assembly.

Acknowledgments: The authors acknowledge financial support from the Projects of International Cooperation and Exchanges (Nos. 2010DFB32980 and 2013DFB30306), the National Science Foundations of China (Nos. 81201198 and 30973360), and the Peking-Tsinghua Center for Life Sciences.

REFERENCES

1. R. R. Betz, Limitations of autograft and allograft: New synthetic solutions. *Orthopedics* 25, 561 (**2002**).
2. W. L. Grayson, M. Frohlich, K. Yeager, S. Bhumiratana, M. E. Chan, C. Cannizzaro, L. Q. Wan, X. S. Liu, X. E. Guo, and G. Vunjak-Novakovic, Engineering anatomically shaped human bone grafts. *Proc. Natl. Acad. Sci. USA* 107, 3299 (**2010**).
3. J. D. Conway, Autograft and nonunions: Morbidity with intramedullary bone graft versus iliac crest bone graft. *Orthop. Clin. North Am.* 41, 75 (**2010**).
4. S. C. Jin, S. G. Kim, J. S. Oh, S. Y. Lee, E. S. Jang, Z. G. Piao, S. C. Lim, M. A. Jeong, J. S. Kim, J. S. You, S. C. Park, Y. S. Cho, S. S. Yang, and S. K. Yu, A comparative study of bone formation following grafting with different ratios of particle dentin and tricalcium phosphate combinations. *J. Biomed. Nanotechnol.* 9, 475 (**2013**).
5. K. I. Jeong, S. G. Kim, J. S. Oh, S. Y. Lee, Y. S. Cho, S. S. Yang, S. C. Park, J. S. You, S. C. Lim, M. A. Jeong, J. S. Kim, and S. Y. Lee, Effect of platelet-rich plasma and platelet-rich fibrin on peri-implant bone defects in dogs. *J. Biomed. Nanotechnol.* 9, 535 (**2013**).
6. S. Weiner and H. D. Wagner, The material bone: Structure mechanical function relations. *Annu. Rev. Mater. Sci.* 28, 271 (**1998**).
7. M. J. Olszta, X. Cheng, S. S. Jee, R. Kumar, Y. Y. Kim, M. J. Kaufman, E. P. Douglasa, and L. B. Gower, Bone structure and formation: A new perspective. *Mater. Sci. Eng. R* 58, 77 (**2007**).
8. W. Traub, T. Arad, and S. Weiner, Three-dimensional ordered distribution of crystals in turkey tendon collagen fibers. *Proc. Natl. Acad. Sci. USA* 86, 9822 (**1989**).
9. W. J. Landis, K. J. Hodgens, J. Arena, M. J. Song, and B. F. McEwen, Structural relations between collagen and mineral in bone as determined by high voltage electron microscopic tomography. *Microsc. Res. Tech.* 33, 192 (**1996**).
10. W. J. Landis, K. J. Hodgens, M. J. Song, J. Arena, S. Kiyonaga, M. Marko, C. Owen, and B. F. McEwen, Mineralization of collagen may occur on fibril surfaces: Evidence from conventional and high-voltage electron microscopy and three-dimensional imaging. *J. Struct. Biol.* 117, 24 (**1996**).
11. W. Zhang, S. S. Liao, and F. Z. Cui, Hierarchical self-assembly of nano-fibrils in mineralized collagen. *Chem. Mater.* 15, 3221 (**2003**).
12. X. Lin, X. Li, H. Fan, X. Wen, J. Lu, and X. Zhang, *In situ* synthesis of bone-like apatite/collagen nano-composite at low temperature. *Mater. Lett.* 58, 3569 (**2004**).
13. D. Lickorish, J. A. Ramshaw, J. A. Werkmeister, V. Glattauer, and C. R. Howlett, Collagen-hydroxyapatite composite prepared by biomimetic process. *J. Biomed. Mater. Res. A* 68, 19 (**2004**).
14. S. Liao, F. Watari, M. Uo, S. Ohkawa, K. Tamura, W. Wang, and F. Cui. The preparation and characteristics of a carbonated hydroxyapatite/collagen composite at room temperature. *J. Biomed. Mater. Res. B Appl. Biomater.* 74, 817 (**2005**).
15. A. Yokoyama, M. Gelinsky, T. Kawasaki, T. Kohgo, U. Konig, W. Pompe, and F. Watari, Biomimetic porous scaffolds with

high elasticity made from mineralized collagen—An animal study. *J. Biomed. Mater. Res. B Appl. Biomater.* 75, 464 (**2005**).
16. F. Cui, Y. Li, and J. Ge, Self-assembly of mineralized collagen composites. *Mater. Sci. Eng. R* 57, 1 (**2007**).
17. J. C. Goes, S. D. Figueiro, A. M. Oliveira, A. A. Macedo, C. C. Silva, N. M. Ricardo, and A. S. Sombra, Apatite coating on anionic and native collagen films by an alternate soaking process. *Acta Biomater.* 3, 773 (**2007**).
18. G. R. Cointry, R. F. Capozza, M. A. Chiappe, S. Feldman, M. D. Meta, S. M. Daniele, N. M. Fracalossi, P. Reina, and J. L. Ferretti, Novel experimental effects on bone material properties and the pre- and postyield behavior of bones may be independent of bone mineralization. *J. Bone Miner. Metab.* 23, 30 (**2005**).
19. H. Gao, B. Ji, I. L. Jager, E. Arzt, and P. Fratzl, Materials become insensitive to flaws at nanoscale: Lessons from nature. *Proc. Natl. Acad. Sci. USA* 100, 5597 (**2003**).
20. M. Balooch, S. Habelitz, J. H. Kinney, S. J. Marshall, and G. W. Marshall, Mechanical properties of mineralized collagen fibrils as influenced by demineralization. *J. Struct. Biol.* 162, 404 (**2008**).
21. Y. Liu, N. Li, Y. P. Qi, L. Dai, T. E. Bryan, J. Mao, D. H. Pashley, and F. R. Tay, Intrafibrillar collagen mineralization produced by biomimetic hierarchical nanoapatite assembly. *Adv. Mater.* 23, 975 (**2011**).
22. Y. Liu, Y. K. Kim, L. Dai, N. Li, S. O. Khan, D. H. Pashley, and F. R. Tay, Hierarchical and non-hierarchical mineralisation of collagen. *Biomaterials* 32, 1291 (**2011**).
23. Y. Liu, S. Mai, N. Li, C. K. Yiu, J. Mao, D. H. Pashley, and F. R. Tay, Differences between top-down and bottom-up approaches in mineralizing thick, partially demineralized collagen scaffolds. *Acta Biomater.* 7, 1742 (**2011**).
24. S. W. Tsai, C. C. Chen, P. L. Chen, and F. Y. Hsu, Influence of topography of nanofibrils of three-dimensional collagen gel beads on the phenotype, proliferation, and maturation of osteoblasts. *J. Biomed. Mater. Res. A* 91, 985 (**2009**).
25. S. W. Tsai, H. M. Liou, C. J. Lin, K. L. Kuo, Y. S. Hung, R. C. Weng, and F. Y. Hsu, MG63 osteoblast-like cells exhibit different behavior when grown on electrospun collagen matrix versus electrospun gelatin matrix. *PLoS One* 7, e31200 (**2012**).
26. R. Ravichandran, J. R. Venugopal, S. Sundarrajan, S. Mukherjee, and S. Ramakrishna, Precipitation of nanohydroxyapatite on PLLA/PBLG/collagen nanofibrous structures for the differentiation of adipose derived stem cells to osteogenic lineage. *Biomaterials* 33, 846 (**2012**).
27. X. Li, J. Xie, J. Lipner, X. Yuan, S. Thomopoulos, and Y. Xia, Nanofiber scaffolds with gradations in mineral content for mimicking the tendon-to-bone insertion site. *Nano Lett.* 9, 2763 (**2009**).
28. B. Pittenger, N. Erina, and C. Su, Quantitative mechanical property mapping at the nanoscale with PeakForce QNM. Bruker Application Note #128 (**2011**).
29. B. V. Derjaguin, V. M. Muller, and Y. P. Toporov, Effect of contact deformations on the adhesion of particles. *J. Colloid Interf. Sci.* 53, 314 (**1975**).
30. L. T. Nguyen, S. Liao, S. Ramakrishna, and C. K. Chan, The role of nanofibrous structure in osteogenic differentiation of human mesenchymal stem cells with serial passage. *Nanomedicine (Lond).* 6, 961 (**2011**).
31. R. M. Blitz and E. D. Pellegrino, The Chemical Anatomy of Bone I. A comparative study of bone composition in sixteen vertebrates. *J. Bone Joint Surg. Am.* 51, 456 (**1969**).
32. C. Liao, F. Lin, K. Chen, and J. Sun, Thermal decomposition and reconstitution of hydroxyapatite in air atmosphere. *Biomaterials* 20, 1807 (**1999**).
33. A. Bigi, A. Ripamonti, G. Cojazzi, G. Pizzuto, N. Roveri, and M. H. Koch, Structural analysis of turkey tendon collagen upon removal of the inorganic phase. *Int. J. Biol. Macromol.* 13, 110 (**1991**).
34. N. Shanmugasundaram, T. Ravikumar, and M. Babu, Comparative physico-chemical and *in vitro* properties of fibrillated collagen scaffolds from different sources. *J. Biomater. Appl.* 18, 247 (**2004**).
35. L. F. Lozano, M. A. Pena-Rico, A. Heredia, J. Ocotlan-Flores, A. Gomez-cortes, R. Velazquez, I. A. Belio, and L. Bucio, Thermal analysis study of human bone. *J. Mater. Sci.* 38, 4777 (**2003**).
36. Q. Wang, S. Jamal, M. S. Detamore, and C. Berkland, PLGA-chitosan/PLGA-alginate nanoparticle blends as biodegradable colloidal gels for seeding human umbilical cord mesenchymal stem cells. *J. Biomed. Mater. Res. A* 96, 520 (**2011**).
37. Q. Wang, J. X. Wang, Q. H. Lu, M. S. Detamore, and C. Berkland, Injectable PLGA based colloidal gels for zero-order dexamethasone release in cranial defects. *Biomaterials* 31, 4980 (**2010**).
38. H. Sahana, D. K. Khajuria, R. Razdan, D. R. Mahapatra, M. R. Bhat, S. Suresh, R. R. Rao, and L. Mariappan, Improvement in bone properties by using risedronate adsorbed hydroxyapatite novel nanoparticle based formulation in a rat model of osteoporosis. *J. Biomed. Nanotechnol.* 9, 193 (**2013**).
39. J. B. Lee, H. N. Park, W. K. Ko, M. S. Bae, D. N. Heo, D. H. Yang, and K. Kwon, Poly(L-lactic acid)/hydroxyapatite nanocylinders as nanofibrous structure for bone tissue engineering scaffolds. *J. Biomed. Nanotechnol.* 9, 424 (**2013**).
40. A. E. Mercado, J. Ma, X. He, and E. Jabbari, Release characteristics and osteogenic activity of recombinant human bone morphogenetic protein-2 grafted to novel self-assembled poly(lactide-co-glycolide fumarate) nanoparticles. *J. Control Release* 140, 148 (**2009**).
41. P. C. Bessa, R. Machado, S. Nürnberger, D. Dopler, A. Banerjee, A. M. Cunha, J. C. Rodríguez-Cabello, H. Redl, M. van Griensven, R. L. Reis, and M. Casal, Thermoresponsive self-assembled elastin-based nanoparticles for delivery of BMPs. *J. Control. Release* 142, 312 (**2010**).
42. J. Kundu, Y. I. Chung, Y. H. Kim, G. Tae, and S. C. Kundu, Silk fibroin nanoparticles for cellular uptake and control release. *Int. J. Pharm.* 388, 242 (**2010**).
43. K. S. Oh, J. Y. Song, S. J. Yoon, Y. Park, D. Kim, and S. H. Yuk, Temperature-induced gel formation of core/shell nanoparticles for the regeneration of ischemic heart. *J. Control. Release* 146, 207 (**2010**).
44. J. H. Park, S. Kwon, J. O. Nam, R. W. Park, H. Chung, S. B. Seo, I. S. Kim, I. C. Kwon, and S. Y. Jeong, Self-assembled nanoparticles based on glycol chitosan bearing 5b-cholanic acid for RGD peptide delivery. *J. Control Release* 95, 579 (**2004**).
45. B. Büyüktimkin, Q. Wang, P. Kiptoo, J. M. Stewart, C. Berkland, and T. J. Siahaan, Vaccine-like controlled-release delivery of an immunomodulating peptide to treat experimental autoimmune encephalomyelitis. *Mol. Pharm.* 9, 979 (**2012**).
46. K. R. Remya, J. Joseph, S. Mani, A. John, H. K. Varma, and P. Ramesh, Nanohydroxyapatite incorporated electrospun polycaprolactone/polycaprolactone-polyethyleneglycol-polycaprolactone blend scaffold for bone tissue engineering applications. *J. Biomed. Nanotechnol.* 9, 1483 (**2013**).
47. K. T. Shalumon, S. Sowmya, D. Sathish, K. P. Chennazhi, S. V. Nair, and R. Jayakumar, Effect of incorporation of nanoscale bioactive glass and hydroxyapatite in PCL/chitosan nanofibers for bone and periodontal tissue engineering. *J. Biomed. Nanotechnol.* 9, 430 (**2013**).
48. P. R. Sreerekha, D. Menon, S. V. Nair, and K. P. Chennazhi, Fabrication of fibrin based electrospun multiscale composite scaffold for tissue engineering applications. *J. Biomed. Nanotechnol.* 9, 790 (**2013**).
49. P. Datta, P. Ghosh, K. Ghosh, P. Maity, S. K. Samanta, S. K. Ghosh, P. K. D. Mohapatra, J. Chatterjee, and S. Dhara, *In vitro* ALP and osteocalcin gene expression analysis and *in vivo* biocompatibility of N-methylene phosphonic chitosan nanofibers for bone regeneration. *J. Biomed. Nanotechnol.* 9, 870 (**2013**).

50. W. Chang, X. Mu, X. Zhu, G. Ma, C. Li, F. Xu, and J. Nie, Biomimetic composite scaffolds based mineralization of hydroxyapatite on electrospun calcium-containing poly(vinyl alcohol) nanofibers. *Mater. Sci. Eng. C Mater. Biol. Appl.* 33, 4369 (**2013**).

51. J. Idaszek, M. Zinn, M. Obarzanek-Fojt, V. Zell, W. Swieszkowski, and A. Bruinink, Tailored degradation of biocompatible poly(3-hydroxybutyrate-co-3-hydroxyvalerate)/calcium silicate/poly(lactide-co-glycolide) ternary composites: An *in vitro* study. *Mater. Sci. Eng. C Mater. Biol. Appl.* 33, 4352 (**2013**).

52. A. Aravamudhan, D. M. Ramos, J. Nip, M. D. Harmon, R. James, M. Deng, C. T. Laurencin, X. J. Yu, and S. G. Kumbar, Cellulose and collagen derived micro-nano structured scaffolds for bone tissue engineering. *J. Biomed. Nanotechnol.* 9, 719 (**2013**).

53. D. I. Zeugolis, S. T. Khew, E. S. Yew, A. K. Ekaputra, Y. W. Tong, L. Y. Yung, D. W. Hutmacher, C. Sheppard, and M. Raghunath, Electro-spinning of pure collagen nano-fibres–just an expensive way to make gelatin? *Biomaterials* 29, 2293 (**2008**).

54. G. He, T. Dahl, A. Veis, and A. George, Nucleation of apatite crystals *in vitro* by self-assembled dentin matrix protein 1. *Nat. Mater.* 2, 552 (**2003**).

55. K. Sweers, K. van der Werf, M. Bennink, and V. Subramaniam, Nanomechanical properties of alpha-synuclein amyloid fibrils: A comparative study by nanoindentation, harmonic force microscopy, and Peakforce QNM. *Nanoscale Res. Lett.* 6, 270 (**2011**).

56. S. Hengsberger, A. Kulik, and P. Zysset, Nanoindentation discriminates the elastic properties of individual human bone lamellae under dry and physiological conditions. *Bone* 30, 178 (**2002**).

57. S. R. Elliott and R. A. Robinson, The water content of bone. I. The mass of water, inorganic crystals, organic matrix, and CO_2 space components in a unit volume of the dog bone. *J. Bone Joint Surg. Am.* 39, 167 (**1957**).

58. I. Jager, P. Fratzl, Mineralized collagen fibrils: A mechanical model with a staggered arrangement of mineral particles. *Biophys. J.* 79, 1737 (**2000**).

59. H. S. Gupta, J. Seto, W. Wagermaier, P. Zaslansky, P. Boesecke, and P. Fratzl, Cooperative deformation of mineral and collagen in bone at the nanoscale. *Proc. Natl. Acad. Sci. USA* 103, 17741 (**2006**).

60. S. Lees and E. A. Page, A study of some properties of mineralized turkey leg tendon. *Connect Tissue Res.* 28, 263 (**1992**).

61. C. M. Nielsen-Marsh, R. E. M. Hedges, T. Mann, and M. J. Collins, A preliminary investigation of the application of differential scanning calorimetry to the study of collagen degradation in archaeological bone. *Thermochim. Acta* 365, 129 (**2000**).

62. Y. K. Kim, L. S. Gu, T. E. Bryan, J. R. Kim, L. Chen, Y. Liu, J. C. Yoon, L. Breschi, D. H. Pashley, and F. R. Tay, Mineralisation of reconstituted collagen using polyvinylphosphonic acid/polyacrylic acid templating matrix protein analogues in the presence of calcium, phosphate and hydroxyl ions. *Biomaterials* 31, 6618 (**2010**).

63. Y. K. Kim, S. Mai, A. Mazzoni, Y. Liu, A. Tezvergil-Mutluay, K. Takahashi, K. Zhang, D. H. Pashley, and F. R. Tay, Biomimetic remineralization as a progressive dehydration mechanism of collagen matrices-implications in the aging of resin-dentin bonds. *Acta Biomater.* 6, 3729 (**2010**).

64. S. S. Jee, T. T. Thula, and L. B. Gower, Development of bone-like composites via the polymer-induced liquid-precursor (PILP) process. Part 1: Influence of polymer molecular weight. *Acta Biomater.* 6, 3676 (**2010**).

65. X. B. Yang, H. I. Roach, N. M. P. Clarke, S. M. Howdle, R. Quirk, K. M. Shakesheff, and R. O. Oreffo, Human osteoprogenitor growth and differentiation on synthetic biodegradable structures after surface modification. *Bone* 29, 523 (**2001**).

66. B. Chuenjitkuntaworn, W. Inrung, D. Damrongsri, K. Mekaapiruk, P. Supaphol, and P. Pavasant, Polycaprolactone/hydroxyapatite composite scaffolds: preparation, characterization, and *in vitro* and *in vivo* biological responses of human primary bone cells. *J. Biomed. Mater. Res.* 94, 241 (**2010**).

67. H. Wang, Y. Li, Y. Zuo, J. Li, S. Ma, and L. Cheng, Biocompatibility and osteogenesis of biomimetic nano-hydroxyapatite/polyamide composite scaffolds for bone tissue engineering. *Biomaterials* 28, 3338 (**2007**).

68. N. Fukui, T. Satoa, Y. Kuboki, and H. Aoki, Bone tissue reaction of nano-hydroxyapatite/collagen composite at the early stage of implantation. *Bio-Med. Mater. Eng.* 18, 25 (**2008**).

69. X. H. Xie, X. W. Yu, S. X. Zeng, R. L. Du, Y. H. Hu, Z. Yuan, E. Y. Lu, K. R. Dai, and T. T. Tang. Enhanced osteointegration of orthopaedic implant gradient coating composed of bioactive glass and nanohydroxyapatite. *J. Mater. Sci.: Mater. Med.* 21, 2165 (**2010**).

70. M. F. Young, J. M. Kerr, K. Ibaraki, A. M. Heegaard, and P. G. Robey, Structure, expression, and regulation of the major noncollagenous matrix proteins of bone. *Clin. Orthop. Relat. Res.* 281, 275 (**1992**).

71. H. Yoshimoto, Y. M. Shin, H. Terai, and J. P. Vacanti, A biodegradable nanofiber scaffold by electrospinning and its potential for bone tissue engineering. *Biomaterials* 24, 2077 (**2003**).

72. C. Li, C. Vepari, H. J. Jin, H. Kim, and D. Kaplan, Electrospun silk-BMP-2 scaffolds for bone tissue engineering. *Biomaterials* 27, 3115 (**2006**).

73. E. K. F. Yim, E. M. Darling, K. Kulangara, F. Guilak, and K. W. Leong, Nanotopography-induced changes in focal adhesions, cytoskeletal organization, and mechanical properties of human mesenchymal stem cells. *Biomaterials* 31, 1299 (**2010**).